Transition from core–shell to Janus chemical configuration for bimetallic nanoparticles

Cyril Langlois, Z.L. Li, Jinjiang Yuan, Damien Alloyeau, Jaysen Nelayah, Davide Bochicchio, Riccardo Ferrando, Christian Ricolleau

ARTICLE TYPE

Transition from core-shell to Janus chemical configuration for bimetallic nanoparticles

Cyril Langlois*[a], Ziyou Li[b], Jun Yuan[c], Damien Alloyeau[a], Jaysen Nelayah[a], Davide Bochicchio[d], Riccardo Ferrando[d] and Christian Ricolleau[a]

Received (in XXX, XXX) Xth XXXXXXXXX 20XX, Accepted Xth XXXXXXXXX 20XX
DOI:

In order to determine the possibilities to control the chemical configuration of bimetallic nanoparticles, we have considered CuAg nanoparticles synthesized by physical route as a model in this study. The synthesis was made by pulsed laser deposition under ultra-high vacuum conditions, *via* a sequential deposition procedure. We show that the temperature of the substrate and the absolute quantity of Ag in a particle are the main parameters that drive the chemical configuration. To explain the transition from a core-shell configuration to a Janus configuration as a function of Ag quantity, we have conducted density-functional theory calculations and atomistic molecular dynamics simulations to investigate the stability of this system. The results are presented together with the experimental observations.

1. Introduction

Bimetallic nanoparticles have been a subject of numerous studies due to the increased capabilities for tuning their properties. Compared to monometallic nanoparticles, they have additional degrees of freedom to adjust the magnetic, optical and catalytic properties, by playing with the composition and the chemical configuration.[1-4] Bimetallic nanoparticles can adopt either alloyed or segregated configurations. The alloyed configuration can be either ordered or disordered, accompanied by very different properties. For instance, ordered CoPt nanoparticles present a tetragonal structure which exhibits a high magnetocrystalline anisotropy, whereas disordered nanoparticles are face centered cubic and do not exhibit such anisotropy.[5-7] Another example, in the field of catalysis, is the use of Ru-Pt nanoparticles to remove carbon monoxide from hydrogen obtained from reformatted hydrocarbons. The article from Alayoglu *et al.* illustrates perfectly the distinct properties of particles with different chemical configuration.[8] Core-shell nanoparticles allow to initiate the selective oxidation reaction at lower temperatures compared to their alloyed counterpart, by combining surface strain effect and a modification of the electronic structure of the Pt shell.

Many different segregated chemical arrangements have been identified, including core-shell, onions-like and side-segregated.[9] The latter is referred as Janus particles because of the similarities between this structure, made of two juxtaposed metallic phases, and the two faces of the Roman god symbolizing 'transitions'. These segregated configurations bring new possibilities for obtaining multifunctional particles.[10] One unique object can easily present both magnetic and optical properties. For instance Co-Ag core-shell particles have magnetic properties due to the Co core, while as the same time exhibit a plasmon resonance associated to the Ag shell that can be tuned by varying the ratio between the shell thickness and the core diameter.[11] For the Janus configuration, the idea is no more to protect the core from external reactions. On the contrary, both metals are accessible for interactions with the environment, which makes possible the design of a new class of catalysts. Such adjustments of the properties need a precise control of the structure of the particles and especially of their chemical configuration. This requires significant efforts for controlling the growth of the nanoparticles, either by chemical or physical routes.

It is of fundamental interest to study under which conditions a core-shell growth is favored compared to the Janus configuration. In the present study, we have chosen the Cu-Ag system as a model system to determine the possibilities to control the chemical configuration using a physical route. The synthesis is made by pulsed laser deposition under ultra-high vacuum conditions, *via* a sequential deposition procedure. We show that this particular growth technique is perfectly adapted to obtain segregated bimetallic nanoparticles, with the temperature of the substrate and the absolute quantity of Ag in a particle as the main parameters that drive the chemical configuration. To explain the transition from a core-shell configuration to a Janus configuration as a function of Ag quantity, we have conducted density-functional theory (DFT) calculations and atomistic molecular dynamics simulations to investigate the stability of this system. The results will be presented here together with the experimental observations.

2. Experimental Methods

CuAg nanoparticles were prepared by pulsed laser ablation in a high vacuum deposition chamber, under a residual pressure of 10^{-8} Torr. A KrF excimer laser at 248 nm was used for the synthesis,

with a pulse duration of 25 ns and a repetition rate of 5 Hz. The energy of the pulses was adjusted separately for Ag and Cu depending on their respective ablation threshold. The pulse energy of the laser was 160 mJ for Ag and 210 mJ for Cu. The resulting deposition rates were typically 0.14 nm per minute for Cu and 0.5 nm per minute for Ag. Commercial TEM grids supporting a 10-15 nm thick amorphous carbon film were used as substrate in this study. The temperature of the substrate during the deposition could be adjusted in the range of 20°C to 800°C. The thickness deposited for a given element was measured by an *in situ* quartz crystal monitor that gives the nominal thickness in a continuous thin film approximation. For each sample, we carried out Cu deposition first, immediately followed by Ag deposition. A 10 nm-thick protective layer of amorphous carbon could be optionally deposited on the sample after cooling down to room temperature. Several Cu@Ag samples were synthesized for this study. The 2@1 samples were obtained by deposition of a nominal thickness of 2 nm of Cu followed by deposition of 1 nm of Ag, with the substrate temperature held at 270°C during all the process. With the same scheme, 1@2 samples were also prepared. The 2@1-100 samples were obtained with the same deposition procedure as for 2@1 samples, except the temperature of the substrate for Ag deposition that was decreased to 100°C. For each synthesis, a reference sample of pure Cu was grown under the same conditions, referred as 2@0 sample. When a protective layer of amorphous carbon was deposited, the samples were labeled with the 'ac-' prefix on their name, such as 'ac-2@0', 'ac-2@1', and 'ac-2@1-100' respectively.

Several TEM techniques have been employed in this study: conventional Bright Field imaging (BF), Energy Filtered Imaging (EFTEM), High Resolution imaging (HRTEM) and High Angle Annular Dark Field imaging in scanning mode (HAADF-STEM) on two different transmission electron microscopes operating at 200 kV: a JEOL JEM-2100F (University Paris 6, France) and a FEI Tecnai F20 STEM (University of Birmingham, UK). Elemental maps have been obtained by the three-window technique in EFTEM, and the filtered images at different energies have been aligned using the script developed by Schaffer *et al.*.[12,13] The EFTEM technique is particularly adapted to study the chemical configurations of bimetallic nanoparticles, as we shown in our previous work.[14]

3. Results

3.1. Cu-Ag chemical configuration as a function of substrate temperature and deposited thickness

HAADF-STEM observations have been carried out on 2@0 and 2@1 samples. The microstructural evolution due to the Ag deposition is clearly evidenced in the two micrographs in Fig. 1, together with the size distributions. Size distribution characteristics and the particle density on the substrate are given in Table 1. For sample 2@0, the pure Cu nanoparticles show a round shape, characterized by a size distribution on the substrate centered around 10 nm. For sample 2@1, a bimodal distribution is observed with the mean peak positions at 3 and 12 nm. It is worth noting that, apart from the small particles around 3 nm, the particle density on the substrate is significantly lower than for pure Cu particles, decreasing from 4700 μm^{-2} to 3800 μm^{-2}.

Table 1 Data relative to the particle assemblies of samples 2@0, 2@1 and 1@2 obtained by TEM image thresholding.[15]

Sample	2@0	2@1	1@2
Data from particle distribution			
Particles mean diameter (nm)	9.9	12	11.8
Peak FWHM (nm)	5.3	8.3	6.2
Particle density (particles per µm²)	4700	3800	3700

In order to investigate the chemical configurations that Cu and Ag adopt on the substrate after the complete deposition procedure, EFTEM imaging experiments have been carried out on the 2@1 sample. Figure 2(a) shows the zero-loss BF image of a representative area on sample 2@1. The silver chemical map of the same area is presented in Fig. 2(b). A majority of the nanoparticles presents a core-shell configuration, with a mean shell thickness of 1 nm ± 0.5 nm. From this EFTEM chemical map, it is clear that the small particles of 3 nm are attributed to pure Ag nanoparticles nucleating on their own on the surface, a result confirmed by HRTEM observations. The capping of the Cu core can be evidenced by Moiré fringes on zone-axis particles and previous work on 2@1 samples using electron tomography showed that the 3D shape of the particles was a truncated sphere with aspect ratio of 1.4.[16] Some particles are linked by a silver bridge, showing signs of sintering process at different stages. On Fig. 2(b), the areas labeled **1** and **2** contain a pair of particles joined together by a silver neck with high curvature, suggesting the initial stage of sintering. Particles labeled **3**, **4** and **5** may correspond to a complete sintering, with a convex external shape but isolated copper cores that have not coalesced. The largest core-shell configurations may result from the sintering of particles with the complete coalescence of the Cu cores.

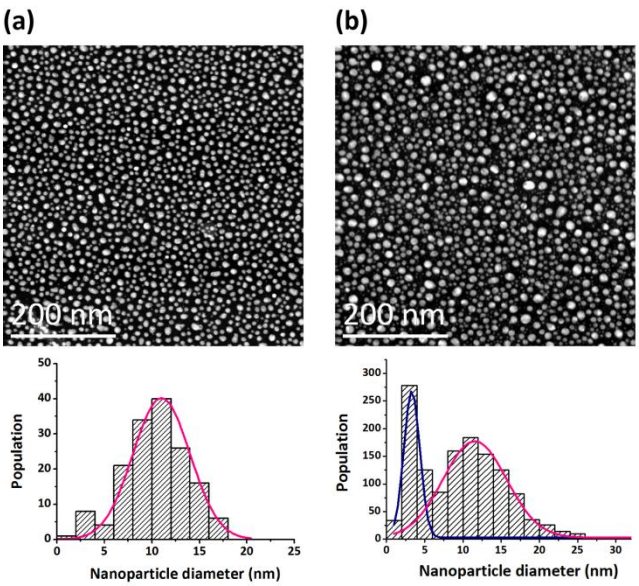

Fig. 1 (Color online) HAADF-STEM images of samples (a) 2@0 Cu and (b) 2@1 CuAg. The size distribution for each micrograph is also presented. Characteristics of the distribution are detailed in Table 1.

The temperature of the substrate can have a strong influence on the chemical configuration of the sample. EFTEM experiments were carried out on 2@1-100 samples. A color chemical map of Cu and Ag on a representative area of the sample is presented in Fig. 3. It is clear that most of the particles are now multi-cores, with Ag bridging several Cu cores inside one large ensemble. Though usually two or three Cu cores are present in one ensemble, up to six Cu cores per ensemble can also be observed, as pointed out by an arrow in Fig. 3. Small core-shell nanoparticles were also formed on 2@1-100 samples, with a circular projection in the substrate plane that likely corresponds to a direct growth of the shell from Ag atoms diffusing on the substrate together with those directly landing on the particle. The large multi-core ensembles were also present in sample 2@1, but in very small proportion (see particles labeled 6 on Fig. 2(b)).

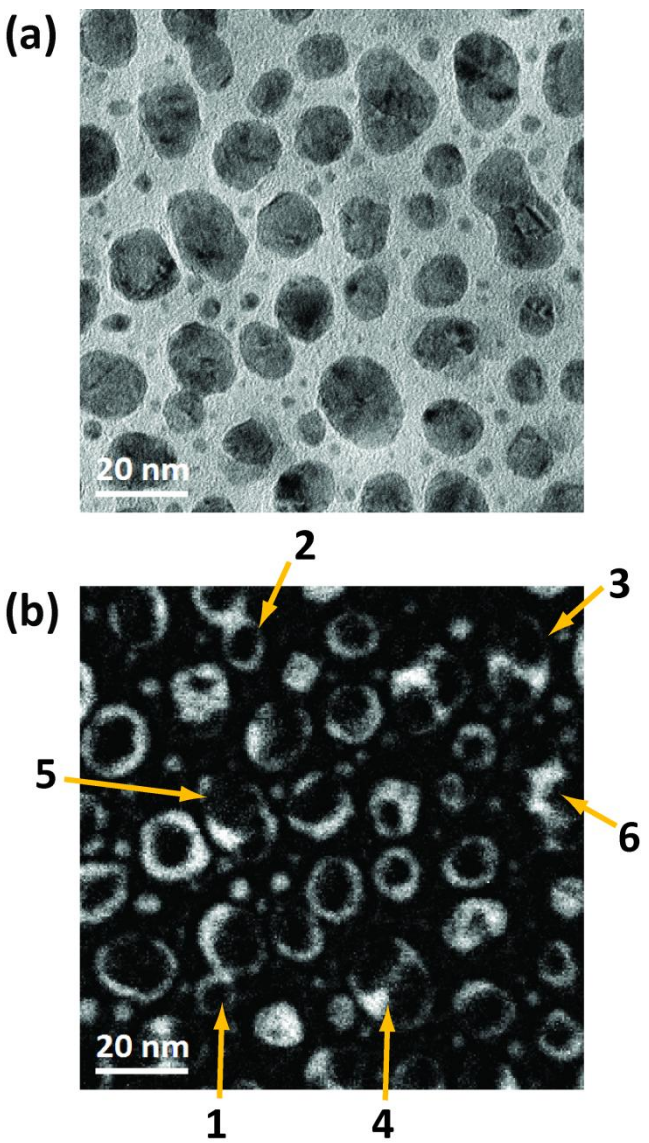

Fig. 2 (Color online) (a) Zero-loss EFTEM image on a representative area of sample 2@1 and (b) Ag elemental map obtained by Energy Filtered TEM on the same area.

To explore the influence of global composition on the chemical configuration of the bimetallic nanoparticles, 1@2 samples have been synthesized. Figure 4 presents the TEM results, with a representative view of the nanoparticles on (a), the size distribution on (b), EFTEM chemical map on (c) and HRTEM on (d). The mean size is around 12 nm (Table 1), very similar to the 2@1 particles with identical total nominal thickness. On the contrary, it is clear from the chemical map of Fig. 4(c) that the chemical configuration is different from that of sample 2@1. A majority of bimetallic particles exhibits a Cu core that is not at the center of the particle, and sometimes touches the outer rim of the particle to form a Janus-like configuration. This is a general tendency over the whole sample, confirmed by high-resolution imaging. A representative example is shown in Fig. 4(d).

3.2. Thermal stability of CuAg system

Thermal stability of the CuAg particles is addressed through annealing experiments under high vacuum of samples ac-2@1-100 and 2@1-100, with and without amorphous carbon capping layer respectively. The temperature of the sample was raised to 550°C and held for 90 min, to allow for a complete evolution of the particle assembly toward equilibrium. Figure 5 shows the initial and final configurations of the ac-2@1-100 sample. The initial configuration is typical of as-grown sample 2@1-100. The post-synthesis deposition of the amorphous carbon did not alter the particles characteristics. Pure Ag nanoparticles were present between the bimetallic particles, the mean diameter of the latter being around 30 nm. The only change after annealing seems to be the disappearance of the small pure Ag nanoparticles. Most grain boundaries visible in the initial configuration were still there after annealing, indicating little changes within the particles.

The same annealing experiment for the uncapped 2@1-100 sample resulted in more pronounced evolution. Figure 6 shows the particle assembly after annealing, in BF imaging (Fig. 6(a)) and EFTEM imaging (Zero-loss (ZL) image in Fig. 6(b) and Ag elemental map in Fig. 6(c)). The size distribution is given in the inset of Fig. 6(a). The mean size of 32 nm and the particle density of 720 μm^{-2} demonstrate a very strong coalescence between the particles. This phenomenon completely altered the initial structure to larger particles, with a typical Janus chemical configuration, that is, with Cu on one side of the particle and Ag on the other side. In most cases, Cu and Ag were separated by a unique planar interface crossing the particle. The planar interfaces could also present an angle, as for the particles #1 in Fig. 6(c).
Here, two distinct structural features are noted: (1) small core-shell nanoparticles were still present on the substrate, under a critical size of 20 nm, and (2) the Cu part of Janus nanoparticles is still surrounded by a thin Ag shell up to 3.5 nm thick.

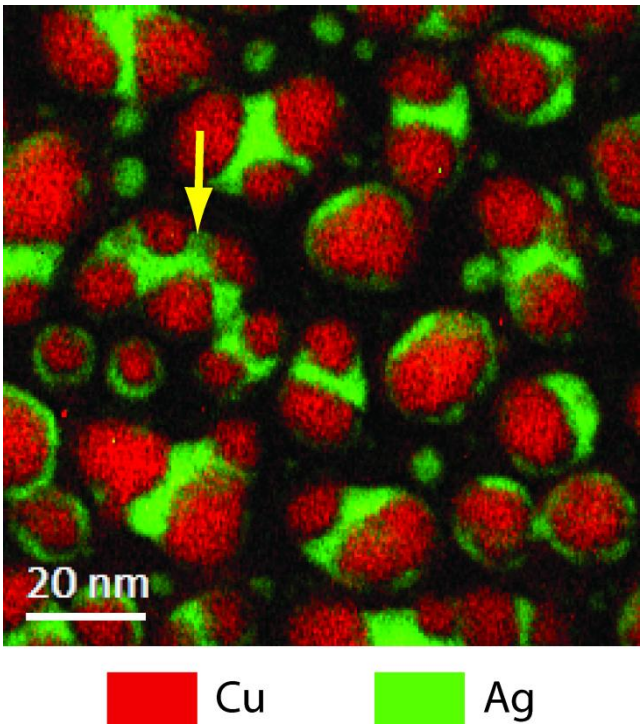

Fig. 3 (Color online) Superimposed Ag and Cu elemental map of sample 2@1-100 obtained by EFTEM using the three-window technique. The arrow designs a CuAg ensemble with six copper cores linked by silver.

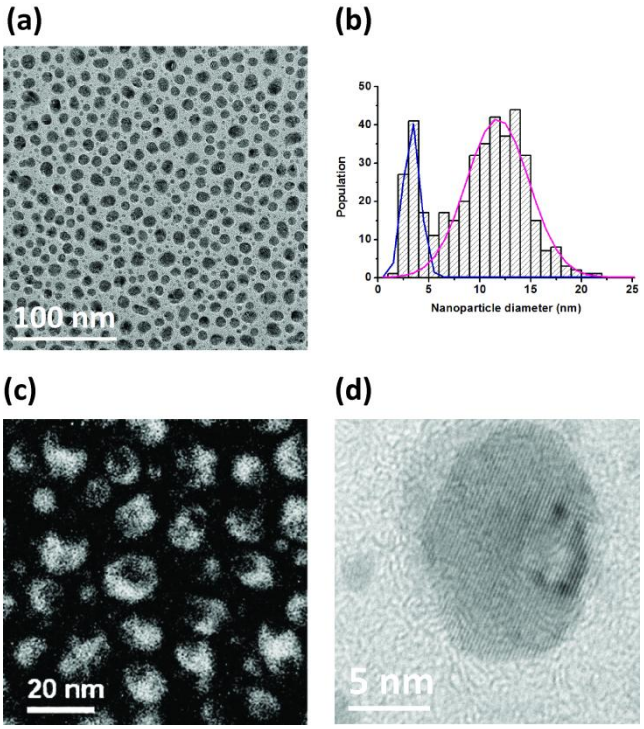

Fig. 4 (Color online) TEM observations of sample 1@2. (a) Bright field TEM image on a representative area of the sample, (b) the size distribution of sample 1@2, (c) Ag elemental map obtained by EFTEM using the three-window technique and (d) HRTEM image of a Janus nanoparticle.

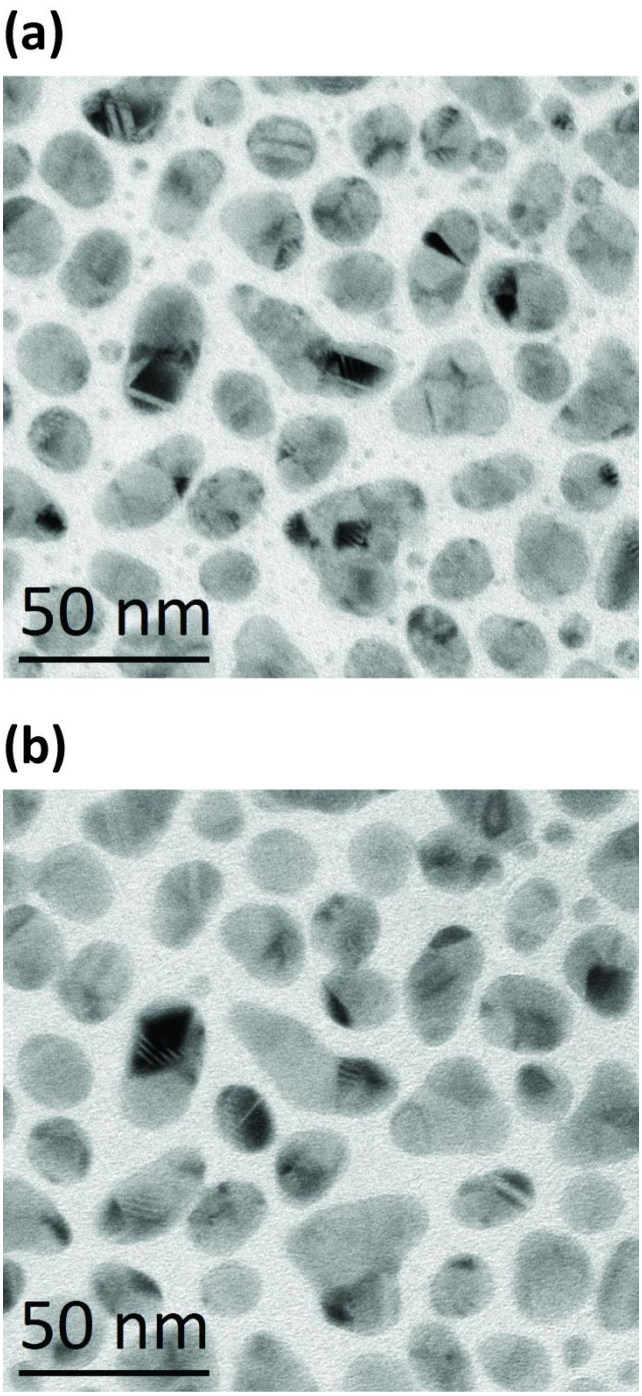

Fig. 5 Annealing experiment on ac-2@1-100 sample: bright field TEM image of (a) the initial configuration and (b) final configuration after 90 min at 550°C.

4. Discussion

4.1. Growth mechanism of the 2@1 microstructure

From the results on samples 2@0 and 2@1, the mechanisms leading to the structural characteristics can be inferred. The decrease of the particle density from $N_1 = 4700$ to $N_2 = 3800$ particles per squared micron due to silver deposition corresponds roughly to $n = 900$ coalescence events per squared micron during the deposition of silver. It means that, assuming only pair-coalescence events of particles, almost 40 % of the existing Cu

particles undergo sintering. Let us consider for simplicity sake that all Cu particles coalescing are initially identical, with the same size d_1 (equal to the mean size of the size distribution of 2@0 sample) and an hemi-spherical morphology (see the model on Fig. 7). The coalescence results theoretically in a double-peak size distribution for Cu cores with peaks positions at d_1 and $2^{1/3}d_1$. The mean size d_2 of the CuAg particles for sample 2@1 should then be:

$$d_2 = \frac{(N_1 - 2n)d_1 + n\sqrt[3]{2}d_1}{N_2} + 2t_s$$

$$= d_1\left[1 + n\left(\frac{\sqrt[3]{2}-1}{N_1 - n}\right)\right] + 2t_s$$

with t_s the Ag shell thickness measured after coalescence. The second term inside the brackets corresponds to the increase percentage compared to the initial size, that is 6%. This leads to a theoretical increase of the mean size to d_2 = 12.6 nm, which corresponds nicely to the effective mean size of the particles in the size distribution on sample 2@1 (see Table 1). On the size distribution, we of course do not see the two theoretical peaks because of the polydispersity of the size distributions. From this analysis, the most probable growth mechanism of the 2@1 core-shell nanoparticles is the formation of an Ag shell around each copper nanoparticles, with pair-coalescence for ~40 % of the particles to give larger core-shell nanoparticles.

One possible driving force for the coalescence to happen is through diffusion of the metallic species on the substrate. To get insight on the first steps of the initial core-shell structure formation, the diffusion of silver and copper on the carbon substrate were lowered, by reducing the substrate temperature for the Ag deposition from 270°C to 100°C. Firstly, we observed that the size distribution and particle density of the Cu cores of the 2@1-100 samples were close to the ones of 2@0 sample. This means that for the 2@1-100 sample, the temperature of 100°C was not sufficiently high to drive the Cu particle diffusion to lead to their coalescence. Secondly, the Ag elemental map reveals that this temperature was not high enough to cause the atomic re-arrangement of the incoming Ag atomic species around the Cu particles. This effect could be related to the high silver deposition rate of 0.5 nm per minute. Here, we can conclude that, at 100°C, the pair-coalescence of particles originates from Ag bridges formed directly during the deposition of silver.

It is worth noting that for other substrates, similar results will be obtained provided that the following general criterion is fulfilled: interactions between the metallic species considered and the substrate must be weak. This is the key point to obtain particles instead of a thin film in the first step of the growth process and to attract the second metallic species around the already formed particles in the second step of the growth. Different metals can exhibit different behavior when interacting with the same substrate.[17] However, the positive point is that an increase of substrate temperature during the growth can overcome metal/substrate interactions to a certain extent and leads to the same kind of nanoparticles.

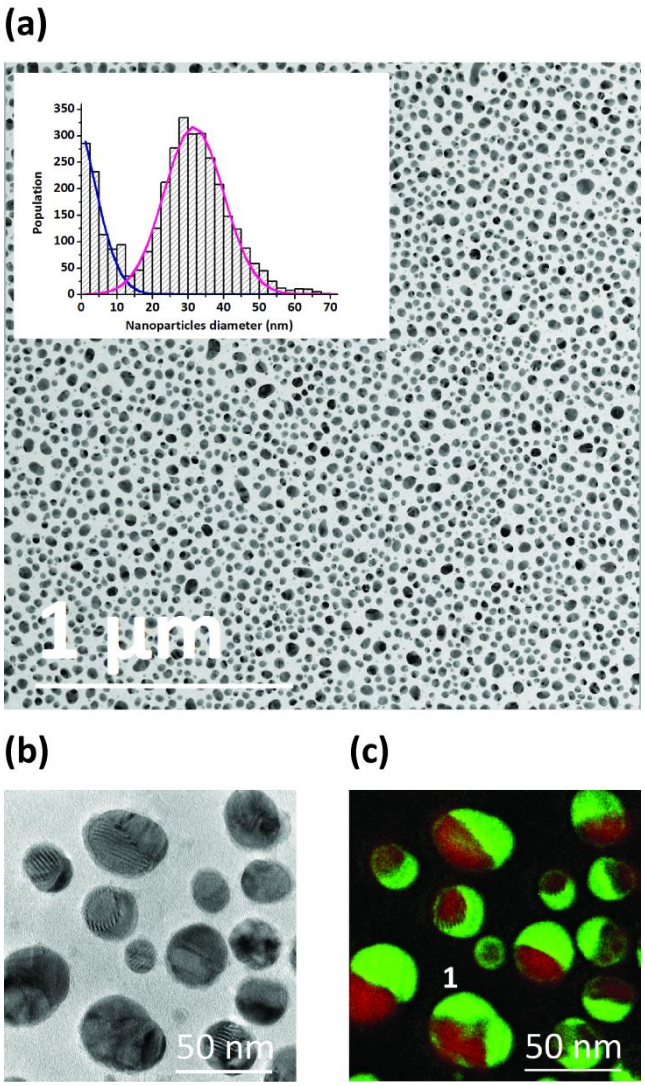

Fig. 6 (Color online) Annealing experiment on 2@1-100 sample. (a) Bright field TEM image of the final configuration of the bimetallic nanoparticles. The inset shows the size distribution of the particles. (b) Zero-loss EFTEM image on a representative area of sample 2@1-100 sample and (c) superimposed Ag and Cu elemental map of sample 2@1-100 obtained by EFTEM using the three-window technique on the same area. Color code identical to Fig. 3.[12,13]

4.2. Diffusion mechanisms in the bimetallic Cu-Ag nanoparticles

It is clear from the annealing results that a capping layer of amorphous carbon completely blocks any coalescence of the particles on the substrate, only allowing the small Ag particles to dissolve themselves in the carbon matrix by Ostwald ripening mechanism. Moreover, no internal re-organization of Cu and Ag inside an initial ensemble was noticed. The latter observation is important because theoretically, the temperature was high enough to induce a chemical re-arrangement by volume diffusion mechanisms of Cu and Ag in the particles.[18] If no re-arrangement is observed, it means that the presence of carbon at the surface blocks the mechanisms responsible for the atomic displacements inside a particle. We could deduce from this that it is mainly the diffusion on the surface of the particle that drives any evolution

of the chemical configuration in the CuAg particles. Another reason could be also that the surface energy of the particles changes due to the carbon matrix, impeding the driving force toward internal re-arrangement with temperature.[19,20] On the contrary, the annealing has a strong effect on the uncapped particles that are free to undergo Ostwald ripening and to coalesce through facile diffusion on the substrate.[21] Without the carbon layer, the coalesced particles can change their chemical arrangement toward Janus configuration. These conclusions are in good agreement with previous simulations carried out on the Cu-Ag system in which the authors show that the surface diffusion processes are energetically favored compared to diffusion inside the core.[22]

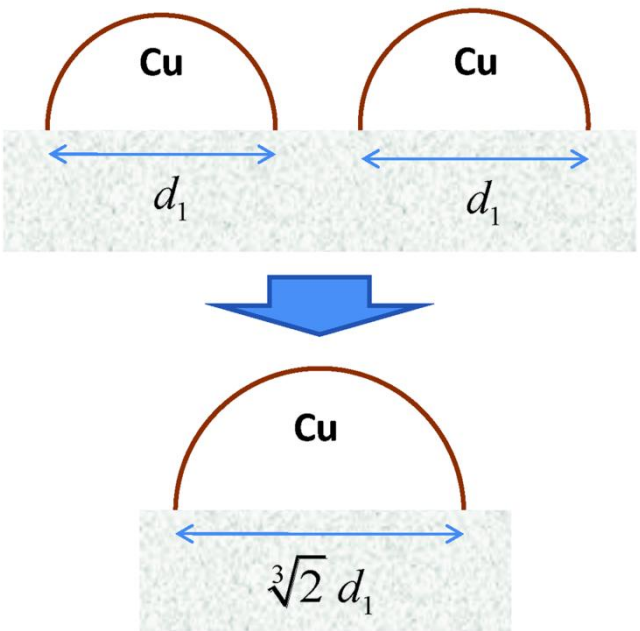

Fig. 7 (Color online) Schematic model showing the result of coalescence of two identical hemispheric Cu particles, with conservation of the total volume of Cu and the hemispherical morphology.

It seems also important to underline that oxidation hardly affects the nanoparticles. The convergence of several strong arguments allows us to rule out the formation of any oxide in the particle, at least in a significant way:

- all the EFTEM experiment on the oxygen threshold that we carried out show very low signal-to-noise ratio and do not evidence the presence of oxide. EELS spectra do not exhibit the typical fine structure of oxidised Cu neither.
- all the HRTEM images acquired on these samples are free of any Cu or Ag oxide lattice fringes, and often show perfect epitaxy between the two metals.
- in case of oxidation of copper, an inversion of the core-shell configuration would be expected, with Ag in the core and Cu oxide as a shell because the mean surface energy of Cu_2O is less than the one of Ag.[23]
- we never noticed any difference between carbon-capped and air-exposed 2@1 sample.

4.3. Competition between core-shell and Janus chemical configuration

It is interesting to note that, although the 2@1 and 1@2 samples are very similar from the point of view of synthesis apart from their chemical composition, the EFTEM characterization reveals a different internal structure of CuAg particles. For the 1@2 sample, not only the average Ag shell thickness is larger as the Ag content increases, but also the core is off-centred and very close to the rim of the particle. These results support the idea that the increase in shell thickness is responsible for the evolution of the chemical configuration toward Janus configuration. This hypothesis can be verified by the annealing experiments. In our annealing experiments, the amount of matter was kept constant (equivalent to 2@1 samples) but coalescence events occurred, resulting in larger particles, hence larger core radius and a larger amount of silver available for re-arrangement around the Cu core. This suggests that both an increase of Ag concentration and a coalescence event have a consequence in common, that is an increase of the amount of silver for a given CuAg particle. Therefore, the Janus configuration identified for the annealed samples may originate from a larger shell thickness that turns finally to the side-segregated configuration, as for the 1@2 samples. From the measurement on the annealed sample and the 1@2 sample, the critical thickness t_c at which the transition occurs from the core-shell to the Janus configuration is estimated to be 3-4 nm. Because of the large size distribution of the particles in the samples, we always find both type of chemical configurations in a given sample. This result is confirmed by measurements carried out on larger CuAg nanoparticles, synthesized by thermal evaporation in a previous work.[14] These particles correspond to a 6@3 system. Both Janus and perfect core-shell nanoparticles are present on the substrate, but for the perfect core-shell configuration, there are no shell with a thickness greater than 4 nm, independently of the Cu core size.

To gain further insight of the driving force for the transition from the core-shell to Janus configuration, we carried out DFT calculations and molecular dynamics simulations (MD) using atomistic potentials derived from second-moment approximation to the tight-binding model. DFT calculations have been made by using the Perdew-Burke-Ernzerhof exchange-correlation functional (PBE) and the Quantum Espresso code.[24] Details are given in the work from Bochiccio *et al.*.[25] We report atomistic calculations by means of two different parameter sets of the Gupta potential.[26] Parametrization P1 has been fitted on DFT calculations of small Ag-Cu clusters,[25] whereas parametrization P2 was fitted on the experimental energetics of single impurities of the bulk host matrix of the other metal.[22] These atomistic potentials have been thoroughly tested against DFT calculations, which showed that P1 agrees very well for what concerns the energetics of core-shell nanoparticles. The agreement of P2 is slightly worse, but the qualitative behaviour is the same for both P1 and P2 (see the supplementary online material of Ref. Bochicchio *et al.*[25]). We have calculated the energetics of single Cu impurities placed inside truncated octahedral Ag clusters (see Fig. 8) in order to determine the most favorable position inside the cluster. We have considered three cluster sizes: 79, 201 and 586 atoms. For the smallest cluster, we performed both DFT and atomistic potential calculations. For 201 and 586 atoms, DFT

calculations become very cumbersome, so that only atomistic calculations were performed. The results are presented in Table 2, with the energies associated to Cu positions under different types of facets. For the $Ag_{78}Cu_1$ the DFT calculations are in good agreement with the results of P2 potential, both showing that for the Cu impurity, the sub-surface positions, just one layer below the surface, are always more stable than central and surface positions. Potential P1 does not agree with DFT and P2 for this size, because it prefers the central positions. For $Ag_{200}Cu_1$ and $Ag_{585}Cu_1$, P2 confirms the tendency to favor sites that are just one layer below the surface. Also P1 does not favor the central sites anymore when size increases. According to P1, the most favorable sites for Cu impurities are located two layers below the surface. Our previous work on the simulation of the Cu-Ag system has shown that, when Cu atoms are deposited on a Ag cluster (inversed deposition model), the Cu atoms agglomerates under the surface in order to form a pure Cu cluster.[27]

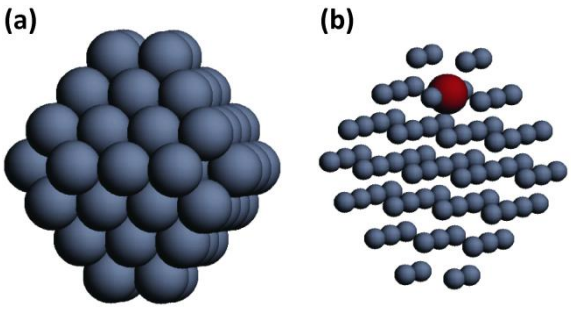

Fig. 8 (Color online) Model for the truncated octahedral $Ag_{78}Cu_1$ cluster used in the DFT, P1 and P2 calculations. The external surface of the $Ag_{78}Cu_1$ cluster is represented in (a). The cluster configuration in (b) represent the Cu atom in the most favorable place according to DFT calculations.

The energy differences between these positions in the cluster are small, so that zero-point energy contribution may be important.[28] However, when the concentration of impurities is finite, the energy differences between aggregates in central and subsurface positions greatly increases. For example, we have considered the truncated octahedron of 201 atoms with 13 Cu atoms. According to P2, the best subsurface position of the Cu aggregate is lower by about 1 eV than the central position of the aggregate. On the contrary, an Ag impurity in a Cu cluster would prefer low-coordination sites, such as vertex sites on the surface. We have verified this for the truncated octahedron of 201 atoms, in which the vertex site is favoured by 0.9 eV compared to central and subsurface sites.

All these results are consistent with the formation of off-center Cu aggregates in Ag-rich clusters. If we consider only the composition inside the particle, it is clear that a low concentration of Ag (i.e. thin Ag shell) corresponds to a core-shell configuration (as clearly shown by the global optimization results[25]) whereas a large concentration of Ag (i.e. a thick Ag shell) should correspond to a Janus configuration.

In order to verify this hypothesis, we have performed global-optimization searches of chemical ordering in Ag-rich clusters. We have considered an fcc truncated octahedron of 586 atoms containing 90% Ag and 10% Cu. We have initially placed the Cu atoms randomly in the cluster and then we have performed extensive global optimization runs in which only exchange moves between atoms of different species were used. The lowest energy configurations according to P1 and P2 are shown in Fig. 9. For both models, an off-center Cu core is obtained so that a quasi-Janus particle is formed. The chemical ordering of these nanoparticles clearly resembles that of the experimental cluster of Fig. 4(d).

Table 2 Results from DFT and atomistic calculations on Ag clusters containing a single Cu atom. For each size, the data report the energy difference from the configuration with Cu on the center of the cluster, which is taken as the zero of energy. Energy differences are given in eV.

Cluster	**Position of the impurity**	**DFT**	**P1**	**P2**
TO_{79}	central sites	0.000	0.000	0.000
	1 layer below (111) facet	-0.001	0.035	-0.046
	1 layer below (100) facet	-0.100	0.109	-0.100
	surface sites on (111) facet	0.136	0.312	0.100
TO_{201}	central sites		0.000	0.000
	1 layer below (111) facet		0.000	-0.035
	1 layer below (100) facet		0.060	-0.067
	2 layers below (100) facet		-0.028	-0.037
TO_{586}	central sites		0.000	0.000
	1 layer below (111) facet		0.010	-0.050
	1 layer below (100) facet		0.047	-0.065
	2 layers below (100) facet		-0.023	-0.030

These simulation results are in good agreement with the experimental observations on the Cu-Ag samples. Moreover, these simulations justify the presence of a thin Ag layer around the Cu part for the Janus nanoparticles. Our results agree with a tendency already observed experimentally in surface science for the Cu growth on Ag (111).[29] In the work from Boquet *et al.*, the authors show that Cu clusters grown on Ag (111) surfaces are covered by one monolayer of silver through segregation effects. It

is worth noting that this result has not been experimentally observed for nanoparticles, even though it is likely to be representative of a quite general behavior. In fact, atomistic simulations are predicting that the same kind of behavior is likely to be observed in AgCo and AgNi too.[30,31]

In order to have a complete view of the problem, it is important to consider also the surface science literature on the CuAg system. A brief review shows that the growth modes of Ag on Cu or Cu on Ag are very different, they strongly depend on the orientation of the substrate, on the substrate temperature and on the amount of matter deposited. The growth of Ag on Cu (111) has been widely studied: although some discrepancy exists, a layer-by-layer growth mode is favoured.[32-34] Twinning has been observed, resulting in similar heteroepitaxy relationships as for the bulk.[35,36] When the Cu substrate is [110] oriented, the growth mode is reported to be layer-by-layer at low temperature, and Stranski-Krastanov at high temperature.[37] For the growth of Cu on Ag, the Stranski-Krastanov growth mode is the most frequently reported.[29,38] From these experimental data, it is clear that the situation is very complex in the case of a nanoparticle because different facets are open to the growth of the shell. Moreover, the sintering between the particles induced by the deposition of silver in the two-step growth procedure makes the comprehension of the final chemical configuration quite complicated. Another complication arises from the fact that the synthesis by pulsed-laser ablation often results in non-equilibrium configurations driven by kinetic effects. The present work highlights the importance of monodispersed nanoparticles and good control of chemical composition in achieving desired structure in bimetallic nanosystems.

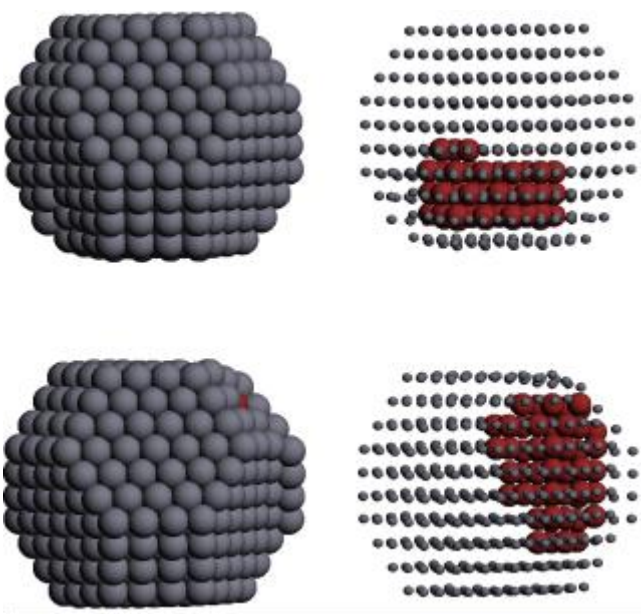

Fig. 9 (Color Online) Structure of a truncated octahedron of 586 containing 90% Ag and 10% Cu after global optimization runs of exchange moves only. The structure is somewhat distorted to release the strain. In the top and bottom row we show the results of P1 and P2, respectively. In both models, quasi-janus configurations are obtained .

5. Conclusion

We have presented in this study the synthesis of bimetallic Cu-Ag nanoparticles *via* pulsed laser ablation, with various chemical compositions. We demonstrated that the deposition of silver on pre-existing copper cores (two-step growth procedure) induced a sintering between the particles, if the substrate temperature was high enough to enable surface diffusion on the substrate. The thermal stability of these nanoparticles has also been studied by annealing experiments under high vacuum conditions. Cu and Ag adopted a segregated chemical configuration, according to the immiscibility of this alloy and the strong difference of their mean surface energy. Two types of segregated configurations were identified: a core-shell configuration for shell thickness under 3 to 4 nm, and a Janus configuration when the amount of Ag inside a particle was in excess compared to this critical thickness. For the Janus configuration, we determined that the Cu part of a particle remains covered by a thin Ag layer. The above observations are supported by DFT calculations and MD simulations, which suggest that the energetically favorite position for a Cu impurity in an Ag cluster is a sub-surface position. These sub-surface impurities can act as seeds for the nucleation of off-center Cu clusters, and lead to the formation of quasi-Janus structures for Ag-rich compositions.

The present work is a step forward to the understanding of the mechanisms leading to the formation of a particular chemical configuration for bimetallic particles. Further studies on the influence of the chemical configuration on the optical properties of such systems are currently under investigation.

Acknoledgments

We are grateful to the Egide (France) and British Council (UK) for supporting this study through the Alliance project, as well as the European COST Action MP0903. R.F. and D.B are grateful for support from CINECA supercomputing center for the project HP10CF1XI1. ZY.L. and J.Y. thank supports from UK EPSRC. We are also grateful to Region Ile-de-France for the support to the JEOL 2100F electron microscope installed at University Paris 6.

Notes and references

[*a] *Laboratoire Matériaux et Phénomènes Quantiques, CNRS-UMR 7162, Université Paris Diderot - Paris 7, Case Courrier 7021, 75205 Paris Cedex 13, France. E-Mail : cyril.langlois@insa-lyon.fr*

[b] *Nanoscale Physics Research Laboratory, School of Physics and Astronomy, University of Birmingham, Birmingham B15 2TT, UK*

[c] *Department of Physics, University of York, Heslington, York YO10 5DD, United Kingdom*

[d] *Dipartimento di Fisica, Università di Genova and IMEM/CNR, Via Dodecaneso 33, 16146 Genova, Italy*

1 L. Guczi, *Catalysis Today*, 2005, **101**, 53-64.

2 K. Major, C. De and S. Obare, *Plasmonics*, 2009, **4**, 61-78.

3 N. S. Sobal, M. Hilgendorff, H. Mahwald, M. Giersig, M. Spasova, T. Radetic and M. Farle, *Nano Letters*, 2002, **2**, 621-624.

4 H. Zeng, S. Sun, J. Li, Z. L. Wang and J. P. Liu, *Applied Physics Letters*, 2004, **85**, 792-794.

5 D. Alloyeau, C. Ricolleau, C. Mottet, T. Oikawa, C. Langlois, Y. Le Bouar, N. Braidy and A. Loiseau, *Nature Materials*, 2009, **8**, 940-946.

6 F. Tournus, N. Blanc, A. Tamion, M. Hillenkamp and V. Dupuis, *Journal of Magnetism and Magnetic Materials*, 2011, **323**, 1868-1872.

7 B. Bian, D. E. Laughlin, K. Sato and Y. Hirotsu, *Journal of Applied Physics*, 2000, **87**, 6962-6964.

8 S. Alayoglu, A. U. Nilekar, M. Mavrikakis and B. Eichhorn, *Nature*, 2008, **7**, 333.

9 R. Ferrando, J. Jellinek and R. L. Johnston, *Chemical Reviews*, 2008, **108**, 845-910.

10 Y. Jin, C. Jia, S.-W. Huang, M. O'Donnell and X. Gao, *Nat Commun*, 2010, **1**, 41.

11 M. Liu and P. Guyot-Sionnest, *Journal of Physical Chemistry B*, 2004, **108**, 5882-5888.

12 L. Reimer, *Energy-Filtering Transmission Electron Microscopy*, Springer Verlag, Berlin, 1995.

13 B. Schaffer, W. Grogger and G. Kothleitner, *Ultramicroscopy*, 2004, **102**, 27-36.

14 C. Langlois, T. Oikawa, P. Bayle-Guillemaud and C. Ricolleau, *Journal of Nanoparticle Research*, 2008, **10**, 997-1007.

15 *Digital Micrograph™*, www.gatan.com/scripting/downloads.php, software by Gatan Inc.

16 M. Valamanesh, C. Langlois, D. Alloyeau, E. Lacaze and C. Ricolleau, *Ultramicroscopy*, 2011, **111**, 149-154.

17 A. A. Schmidt, H. Eggers, K. Herwig and R. Anton, *Surface Science*, 1996, **349**, 301-316.

18 D. B. Butrymowicz, J. R. Manning and M. E. Read, *Journal of Physical and Chemical Reference Data*, 1974, **3**, 527-602.

19 O. M. Løvvik and S. M. Opalka, *Surface Science*, 2008, **602**, 2840-2844.

20 F. Tao, M. E. Grass, Y. Zhang, D. R. Butcher, J. R. Renzas, Z. Liu, J. Y. Chung, B. S. Mun, M. Salmeron and G. A. Somorjai, *Science*, 2008, **322**, 932-934.

21 D. Alloyeau, G. Prévot, Y. Le Bouar, T. Oikawa, C. Langlois, A. Loiseau and C. Ricolleau, *Physical Review Letters*, 2010, **105**, 255901.

22 F. Baletto, C. Mottet and R. Ferrando, *Physical Review B*, 2002, **66**, 155420.

23 D. A. Firmansyah, T. Kim, S. Kim, K. Sullivan, M. R. Zachariah and D. Lee, *Langmuir*, 2009, **25**, 7063-7071.

24 P. Giannozzi, S. Baroni, N. Bonini, M. Calandra, R. Car, C. Cavazzoni, D. Ceresoli, G. L. Chiarotti, M. Cococcioni, I. Dabo, A. Dal Corso, S. De Gironcoli, S. Fabris, G. Fratesi, R. Gebauer, U. Gerstmann, C. Gougoussis, A. Kokalj, M. Lazzeri, L. Martin-Samos, N. Marzari, F. Mauri, R. Mazzarello, S. Paolini, A. Pasquarello, L. Paulatto, C. Sbraccia, S. Scandolo, G. Sclauzero, A. P. Seitsonen, A. Smogunov, P. Umari and R. M. Wentzcovitch, *Journal of Physics: Condensed Matter*, 2009, **21**, 395502.

25 D. Bochicchio and R. Ferrando, *Nano Letters*, 2010, **10**, 4211-4216.

26 R. P. Gupta, *Physical Review B*, 1981, **23**, 6265-6270.

27 F. Baletto, C. Mottet and R. Ferrando, *Physical Review Letters*, 2003, **90**, 135504.

28 H. Yildirim, A. Kara and T. S. Rahman, *Journal of Physics: Condensed Matter*, 2009, **21**, 084220.

29 F. Bocquet, C. Maurel, J.-M. Roussel, M. Abel, M. Koudia and L. Porte, *Physical Review B*, 2005, **71**, 075405.

30 I. Parsina and F. Baletto, *The Journal of Physical Chemistry C*, 2010, **114**, 1504-1511.

31 F. Calvo, E. Cottancin and M. Broyer, *Physical Review B*, 2008, **77**, 121406.

32 Y. Borensztein, T. Lopez-Rios and G. Vuye, *Physical Review B*, 1988, **37**, 6235.

33 U. Kürpick, G. Meister and A. Goldmann, *Applied Surface Science*, 1995, **89**, 383-392.

34 C. Mottet, G. Tréglia and B. Legrand, *Physical Review B*, 1992, **46**, 16018.

35 J. B. Liu, Y. W. Zeng and L. Meng, *Journal of Alloys and Compounds*, 2008, **464**, 168-173.

36 K. Umezawa, S. Nakanishi, M. Yoshimura, K. Ojima, K. Ueda and W. M. Gibson, *Physical Review B*, 2000, **63**, 035402.

37 T. N. Taylor, R. E. Muenchausen and M. A. Hoffbauer, *Surface Science*, 1991, **243**, 65-82.

38 P. A. Huttunen and A. Vehanen, *Physical Review B*, 1990, **42**, 11570.